How light emerges from an illuminated array of subwavelength holes

J. BRAVO-ABAD[1], A. DEGIRON[2], F. PRZYBILLA[2], C. GENET[2], F. J. GARCÍA-VIDAL[1]*, L. MARTÍN-MORENO[3] AND T. W. EBBESEN[2]

[1]Departamento de Física Teórica de la Materia Condensada, Universidad Autónoma de Madrid, E-28049 Madrid, Spain
[2]ISIS, Université Louis Pasteur, 67000 Strasbourg, France
[3]Departamento de Física de la Materia Condensada, Universidad de Zaragoza-CSIC, E-50009 Zaragoza, Spain
*e-mail: fj.garcia@uam.es

Published online: 29 January 2006; doi:10.1038/nphys213

The extraordinary optical transmission through periodic arrays of subwavelength holes has been studied extensively since it was first reported in 1998, owing to both its fundamental implications and its technological potential. The picture of the underlying mechanism that emerges from most of the theoretical studies is a resonant process assisted by surface electromagnetic modes, such as surface plasmons. However, these studies consider an infinite array of holes. By combining experiment and theory, we have analysed the influence of the inherent finite size of the arrays and report here the unexpected spatial distribution of light as it emerges from the arrays. This distribution is strongly anisotropic and extremely sensitive to the angle of incidence of the impinging light. The behaviour can be explained by a model that takes into account the asymmetry induced by the array edges, and the effects this has on the emission pattern across the array.

After the experimental finding of extraordinary optical transmission (EOT) in periodic arrays of subwavelength holes perforated in opaque metal films[1], much work has been devoted to the analysis of their fundamental aspects[2–12]. However, the increasing use of EOT in various applications from sensors to opto electronic devices[13–18] requires further understanding of the phenomenon. In most cases, finite arrays of holes are the standard structures that underlie many such applications. Typically, it is assumed that the back coupling of the surface plasmon to light at the exit surface of the array is uniform across the array. While trying to analyse the effects of finite size on the EOT in hole arrays, we noticed that the emission pattern from the finite arrays is far from uniform. In view of the consequences this can have on the interpretation of EOT results and its optimization for a given purpose, the phenomenon was analysed in detail and modelled to understand the underlying physics.

In order to carry out the experimental analysis, several hole arrays were milled in freestanding Ag films using a focused ion beam. The samples consist of square lattices of $N \times N$ circular holes with a radius a of 135 nm. The period of the lattice, P, is 600 nm and the thickness of the film, h, is 225 nm. A schematic picture of this type of structure is shown in Fig. 1a. In Fig. 1b we show the zero-order transmittance spectrum corresponding to a 31×31 array with a clear resonant peak appearing at a wavelength of around 700 nm.

On the theoretical side, we use a formalism based on a modal expansion of the electromagnetic fields that allows us to deal with an arbitrary collection of indentations perforated on a metallic film[19]. In this theoretical framework, metal regions are treated as perfect conductors. This approximation has semiquantitative value even for real metals at optical wavelengths, provided the hole radius is enlarged by a quantity proportional to the skin depth of the metal[20]. The inset of Fig. 1b shows our theoretical prediction for the total transmittance spectrum for a 31×31 array of holes with the same geometrical parameters as in the experiment. Although the theoretical resonant peak appears at a slightly smaller wavelength (630 nm) than in the experiment, the agreement between the theoretical and experimental spectra is rather good.

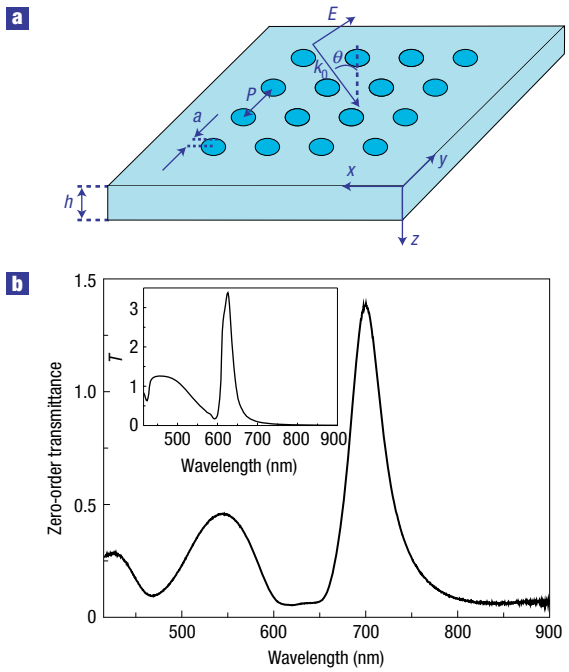

Figure 1 Resonant transmission through a 31 × 31 hole array. a, Schematic view of the structure under study and the corresponding reference system used. Parameters used in the definition of the holes, metal film and incident plane wave are also shown. **b**, Experimental zero-order transmittance through a 31 × 31 hole array defined by $a = 135$ nm, $P = 600$ and $h = 225$ nm. The curve in the inset corresponds to the total transmittance (T) spectrum obtained from numerical simulations.

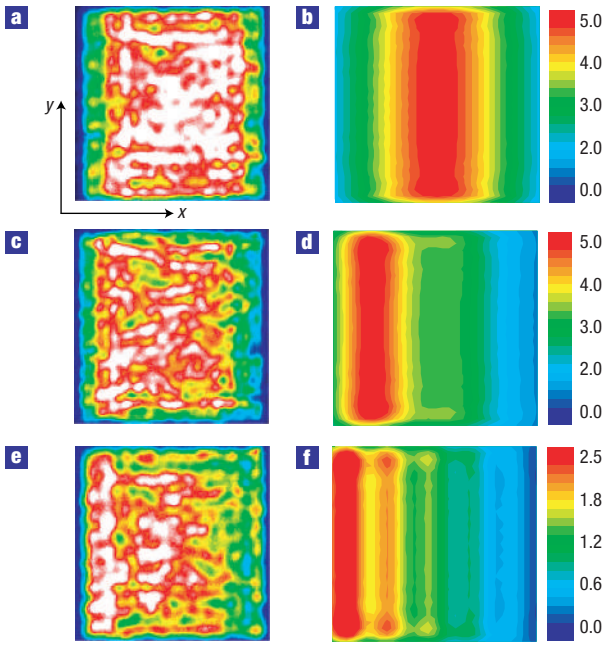

Figure 2 Demonstration of the strong sensitivity of emission patterns to the incident angle. Left panels: Experimental emissivity. Right panels: Theoretical transmission per hole. Patterns are obtained at resonance for a 31 × 31 hole array illuminated by p-polarized light using the same colour scale. The results for three different values of θ are shown: **a**,**b** correspond to $\theta = 0^\circ$, **c**,**d** to $\theta = 2^\circ$ and **e**,**f** to $\theta = 5^\circ$.

Emissivity maps of light emerging from the hole array are measured with a charge-coupled-device camera. The wavelengths of the light incident on the system are selected by a narrow band-pass filter (50 nm) placed between the white light source and the hole array. Figure 2a shows the emissivity map for the case analysed in Fig. 1b with a wavelength filter at 700 nm and normal incident radiation with its electric field E pointing along the x direction. In this case, the emissivity is mainly located in a centred wide strip perpendicular to the incident polarization, and it decays near the borders in the x direction. If the incident angle is slightly changed from $\theta = 0^\circ$ to $\theta = 2^\circ$ (see Fig. 2c), the region where the emission is mainly concentrated moves to the left, that is, it is shifted in the opposite direction to the projection of the incident wavevector, $\mathbf{k}_0$, on the x axis. This displacement is more evident in the case of $\theta = 5^\circ$ (Fig. 2e), where the strip of maximum emission is located almost at the left border of the sample. If the incident angle (pictures not shown here) is further increased, the asymmetry disappears and the emission patterns tend to show an almost uniform spatial distribution. In all cases, the emissivity is practically constant along the y direction, with the presence of borders affecting only the last one or two rows of holes. The asymmetry observed in the emissivity maps is found to be strongly polarization dependent: we have found that the measured pattern is almost independent of θ if the incident light is s-polarized.

In the theoretical framework, the contribution to the total transmittance owing to hole α, T_α, is expressed in terms of the modal amplitudes of the electric field at the input (E_α) and output (E'_α) interfaces of the hole. The set $\{E_\gamma, E'_\gamma\}$ (where γ runs over all the holes in the array) satisfies a set of linear equations (see equation (3) in ref. 19). The quantities T_α can be directly compared to the emissivity maps obtained experimentally. In Fig. 2b,d,f, we plot the calculated T_α (evaluated at resonance), corresponding to the cases Fig. 2a,c,e analysed experimentally. This figure shows that the numerical results confirm the finite size effects and the strong dependence on θ found in the experiments.

In order to understand the physical origin of the emissivity patterns observed in the experiments, it is best to begin with a theoretical analysis of the dependence of T_α on the number of holes. Owing to computer-memory constraints, we are limited to the treatment of square arrays with up to 41 × 41 holes. However, as seen in Fig. 2, the patterns are almost uniform in the y direction for the chosen polarization. Therefore, the spatial distribution of light emerging from the structure in square arrays will be similar to that found in finite arrays in which the number of holes in the y direction (N_y) is taken to infinity. This is confirmed in Fig. 3 where we compare the transmission-per-hole patterns for a 31 × 31 array (blue dots) with that obtained for a 31 × ∞ array (blue curve). Taking the limit $N_y \to \infty$ allows the use of Bloch's theorem, thus greatly enlarging the number of holes in the x direction (N_x) that can be treated within our theoretical approach.

Figure 3 shows T_α evaluated at resonance for normal incident p-polarized radiation for arrays with N_x varying from $N_x = 11$ up to $N_x = 151$. The geometrical parameters of these rectangular arrays are the same as those analysed previously ($a = 135$ nm, $P = 600$ nm and $h = 225$ nm). Two regimes can be clearly distinguished. For small N_x (up to $N_x = 31$), T_α is maximum at the centre of the array. On the other hand, for large-enough N_x the pattern consists of an almost uniform central part (with some oscillations around the value obtained for $N_x \to \infty$) and two edge regions where the spatial distribution (measured from their respective edges) is virtually independent of N_x.

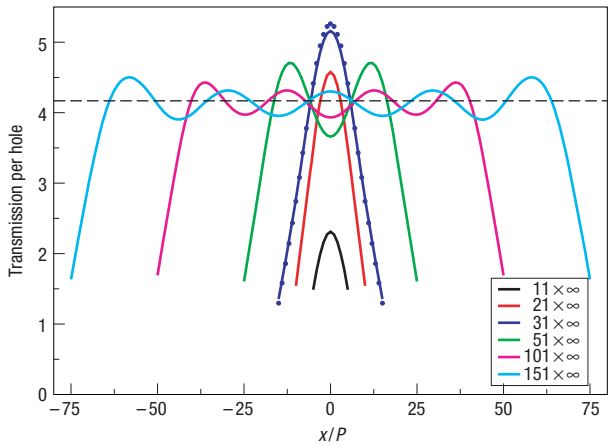

Figure 3 Evolution of the transmission per hole as N_x is increased. Transmission per hole along the x axis computed at the corresponding resonant wavelength for $N_x \times \infty$ hole arrays. Normal incident p-polarized radiation is assumed and the geometrical parameters are as in Fig. 1. The dashed line shows the result for an infinite periodic array of holes. Blue dots correspond to a cut along the central row of a 31 × 31 array (see Fig. 1b).

To understand the role of the edges in the transmission for a large system, it is convenient to start with a formulation that shows explicitly the response of the infinite array. Given that the set of equations that obey the modal amplitudes $\{E_\alpha, E'_\alpha\}$ is linear, these magnitudes can be obtained from

$$E_\alpha = \sum_{\beta \in A} f_{\beta\alpha}, \qquad E'_\alpha = \sum_{\beta \in A} f'_{\beta\alpha}, \tag{1}$$

where $f_{\beta\alpha}$ ($f'_{\beta\alpha}$) behaves as a Green function that gives the modal amplitude of the E-field at the input (output) interface of the hole α when the hole β within the array (A) is illuminated. Importantly, $f_{\beta\alpha}$ and $f'_{\beta\alpha}$ must be computed self-consistently, that is, by taking into account the presence of all the other holes in the array t different from α and β.

The corresponding modal amplitudes for an infinite array $\{E^\infty_\alpha, E'^\infty_\alpha\}$ can be also extracted from f^∞ and f'^∞, where the superscript ∞ means that these basic magnitudes need to be calculated for an infinite array. Therefore, it is possible to recover the surface modes (both proper bound states and leaky modes) that exist in periodically corrugated surfaces and that are responsible for EOT from the knowledge of f and f'. We want to stress here that the local vision provided by f and f' does not give additional information on the origin of EOT. However, as we will see below, this local vision is a complementary point of view that is more suitable when the symmetry of the infinite system is reduced, for instance, when the array is finite (as in the case analysed in this paper) and/or when the structure is not illuminated by a plane wave.

As said before, we are interested in expressing the modal amplitude associated with the hole α in the finite array, E_α, as E^∞_α plus a contribution due to the presence of the two edges. For this purpose, first we divide the sum over illuminated holes yielding E^∞_α into three terms (see the schematic picture in Fig. 4): one coming from the holes belonging to the finite array analysed ($E^A_\alpha = \sum_{\beta \in A} f^\infty_{\beta\alpha}$) and two reflecting the contributions of the left ($E^L_\alpha = \sum_{\mu \in L} f^\infty_{\mu\alpha}$) and right ($E^R_\alpha = \sum_{\gamma \in R} f^\infty_{\gamma\alpha}$) regions needed to complete the finite system and convert it into an infinite system. Second, by adding/subtracting E^∞_α to/from E_α given by

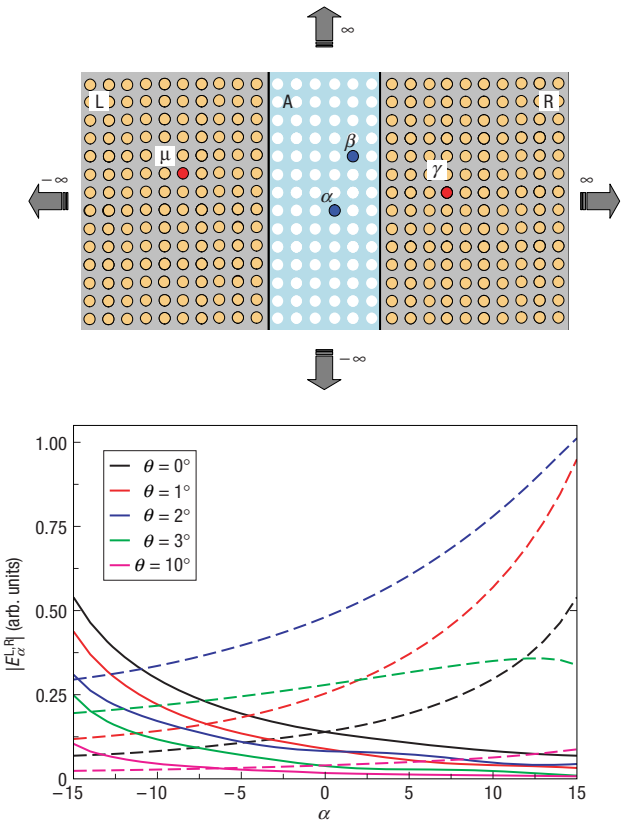

Figure 4 Effects of the array edges on the emissivity from the hole array. Top panel: Schematic picture of the theoretical model used to describe the transmission per hole features of a finite array of subwavelength holes. Bottom panel: $|E^L_\alpha|$ (full curves) and $|E^R_\alpha|$ (dashed curves) as a function of the object label α in a 31 × ∞ array for several angles of incidence.

equation (1), we can end up with an expression for E_α:

$$E_\alpha = E^\infty_\alpha - E^L_\alpha - E^R_\alpha + \sum_{\beta \in A} (f_{\beta\alpha} - f^\infty_{\beta\alpha}), \tag{2}$$

and a similar expression for E'_α. Importantly, all this mathematical manipulation has led us to three edge contributions in equation (2) that have physical meaning. $S_\alpha \equiv \sum_{\beta \in A}(f_{\beta\alpha} - f^\infty_{\beta\alpha})$ takes into account the fact that the self-consistent electromagnetic fields in the finite array are different from the infinite case, owing to the presence of the two edges. Its Fourier transform presents two peaks located at $k_{0x} = k_0 \sin\theta$ and $-k_{0x}$ (with $k_0 = 2\pi/\lambda$, λ being the wavelength of the incident light), indicating that this term is related to the reflections at the borders of the array of the running surface waves, responsible for EOT in infinite arrays. The interference between these surface waves provokes the appearance of oscillations in the transmission per hole patterns for large arrays, as can be seen in Fig. 3. On the other hand, E^L_α and E^R_α represent the lack of emitters contributing to the self-consistent formation of the surface electromagnetic modes previously mentioned. These contributions are expressed as negative illumination coming from phantom holes located at the left and right regions of the finite array. We have checked that, for small arrays, the dominant edge contributions are just E^L_α and E^R_α, whereas the term S_α is important when the hole array is large. As we are interested in explaining the spatial distribution of a 31 × 31 array, we now concentrate on E^L_α and E^R_α.

In the bottom panel of Fig. 4 we show the behaviour of the moduli of E_α^{L} and E_α^{R} evaluated at resonance as a function of the hole location α for a $31 \times \infty$ array with the same geometrical parameters as used in previous calculations and for different angles of incidence. For normal incidence (black curves), $|E_\alpha^{\mathrm{L}}|$ is maximum at the left end of the array and decays as the hole α is separating from the left border with a typical decay length (L_{D}) that is of the order of 10–15 times the period of the array. A similar behaviour is observed for $|E_\alpha^{\mathrm{R}}|$, explaining why the transmission per hole pattern for a $31 \times \infty$ array at 0° is maximum at the centre. For larger arrays (much larger than this L_{D}), the regions close to the edges of the array would present a similar trend but the influence of these terms in the central part of the array is severely reduced. As the scattering cross-section of a hole depends strongly on its diameter[5], so does L_{D}. As a consequence, if the diameter of the hole is very small in comparison with the resonant wavelength (that is, roughly the period of the array), a very large number of holes are necessary in order to obtain the transmittance values predicted for infinite arrays.

The edge contributions ($|E_\alpha^{\mathrm{L}}|$ and $|E_\alpha^{\mathrm{R}}|$) are very different already for small angles of incidence (see Fig. 4), explaining why the observed emissivity is concentrated on one side of the array for such small angles. When the angle of incidence is large enough ($\theta \approx 10°$) the two contributions are again comparable, resulting in the uniform pattern also observed in the experiments. This angle dependence can be traced back to the behaviour of $f_{\gamma\alpha}^{\infty}$. As stated before, $f_{\gamma\alpha}^{\infty}$ represents the response of the system to local illumination (that is, the in-plane wavevector is not well defined), so it contains the behaviour of all surface electromagnetic waves. This results in a complex behaviour of $f_{\gamma\alpha}^{\infty}$ at short distances, whereas at large distances the spatial dependence of this quantity is that of a wave. As a first approximation, which gives a better insight into the underlying physics, we can express $f_{\gamma\alpha}^{\infty} = |f_{\gamma\alpha}^{\infty}| \mathrm{e}^{ik_0 x_\gamma} \mathrm{e}^{ik_0 |x_\gamma - x_\alpha|}$ for $\gamma \neq \alpha$, and $f_{\gamma\gamma}^{\infty} = |f_{\gamma\gamma}^{\infty}| \mathrm{e}^{ik_0 x_\gamma} \mathrm{e}^{i\phi}$, where ϕ is a wavelength-dependent phase. When incorporating these magnitudes into E_α^{R} and E_α^{L}, we obtain

$$E_\alpha^{\mathrm{R}} \approx \mathrm{e}^{-ik_0 x_\alpha} \sum_{\gamma \in \mathrm{R}} |f_{\gamma\alpha}^{\infty}| \mathrm{e}^{i(k_{0x}+k_0)x_\gamma} \tag{3}$$

$$E_\alpha^{\mathrm{L}} \approx \mathrm{e}^{ik_0 x_\alpha} \sum_{\mu \in \mathrm{L}} |f_{\mu\alpha}^{\infty}| \mathrm{e}^{i(k_{0x}-k_0)x_\mu} . \tag{4}$$

In order to fully understand the behaviour in a finite array, we find it convenient to consider first what occurs when an infinite array is illuminated by a normal-incident plane wave. In this case, regions R and L in equations (3) and (4) are understood as the regions to the right and left of site α, respectively. In this way, E_α^{∞} can be written down as $E_\alpha^{\infty} = E_\alpha^{\mathrm{L}} + E_\alpha^{\mathrm{R}} + f_{\alpha\alpha}^{\infty}$. At $\lambda = P$, all terms in $E_\alpha^{\mathrm{R,L}}$ interfere constructively at site α, but not in phase with the term $f_{\alpha\alpha}^{\infty}$. The optimal interference between all these terms occurs then at a resonant wavelength λ_{M} slightly larger than P, marking the appearance of a surface electromagnetic mode (Bloch wave), which is responsible for the EOT phenomenon. Notice that, at $\lambda = \lambda_{\mathrm{M}}$, the interference of all $f_{\gamma\alpha}^{\infty}$ in $E_\alpha^{\mathrm{R,L}}$ (equations (3) and (4)) is not fully constructive, that is, when travelling from a site to its closest neighbour the wave accumulates a phase $\Delta_{\mathrm{SW}} = k_0 P$ different from 2π. Let us now consider the finite array, with the definitions for L and R regions as sketched in Fig. 4. At $\lambda = \lambda_{\mathrm{M}}$, the interference of terms $f_{\gamma\alpha}^{\infty}$ with $\gamma \neq \alpha$ can be improved by tilting the incident wave, therefore adding to Δ_{SW} the 'optical path' phase $\Delta_{\mathrm{OP}} = k_{0x} P$, accumulated by the incoming plane wave before reaching the holes. As surface modes appear close to the light line, k_{0x} (and therefore the tilt angle) for optimal interference is very small. However, given that the total phase difference between nearest neighbours is either $\Delta_{\mathrm{OP}} + \Delta_{\mathrm{SW}}$ (for E_α^{R}) or $\Delta_{\mathrm{OP}} - \Delta_{\mathrm{SW}}$ (for E_α^{L}), when one of the edge contributions is optimized, the other one degrades. When k_{0x} is increased away from the optimal value, both $\Delta_{\mathrm{OP}} + \Delta_{\mathrm{SW}}$ and $\Delta_{\mathrm{OP}} - \Delta_{\mathrm{SW}}$ depart from 2π, explaining why the resonant behaviour is lost already for moderate angles of incidence. To summarize, the whole phenomenology found for the emission pattern in finite arrays originates from a delicate balance between the optical path phase and that of surface waves coming from the edges.

Light emerges from the surface of finite hole arrays in an asymmetric pattern, which, unexpectedly, depends strongly on the angle of incidence, even for very small angles. The experimental results can be very well fit to a theoretical model in which the properties of a finite array are obtained as the corresponding properties for an infinite array plus the contribution coming from electromagnetic waves launched by the edges. The analysis of these waves explains all phenomenology found both in the experiments and in the numerical simulations, thus providing further insight onto the EOT phenomenon that will be crucial when designing arrays and interpreting the results in a variety of applications, such as enhancing spectroscopy signals, subwavelength lithography and optical devices.

Received 2 August 2005; accepted 21 December 2005; published 29 January 2006.

References

1. Ebbesen, T. W., Lezec, H. J., Ghaemi, H. F., Thio, T. & Wolff, P. A. Extraodinary optical transmission through sub-wavelength hole arrays. *Nature* **391,** 667–669 (1998).
2. Popov, E., Nevière, M., Enoch, S. & Reinisch, R. Theory of light transmission through subwavelength periodic hole arrays. *Phys. Rev. B* **62,** 16100–16108 (2000).
3. Martín-Moreno, L. *et al.* Theory of extraodinary optical transmission through subwavelength hole arrays. *Phys. Rev. Lett.* **86,** 1114–1117 (2001).
4. Collin, S., Pardo, F., Teissier, R. & Pelouard, J. L. Strong discontinuities in the complex photonic band structure of transmission metallic gratings. *Phys. Rev. B* **63,** 033107 (2001).
5. Müller, R., Malyarchuk, V. & Lienau, C. Three-dimensional theory on light-induced near-field dynamics in a metal film with a periodic array of nanoholes. *Phys. Rev. B* **68,** 205415 (2003).
6. Sarrazin, M., Vigneron, J.-P. & Vigoureux, J.-M. Role of Wood anomalies in optical properties of thin metallic films with a bidimensional array of subwavelength holes. *Phys. Rev. B* **67,** 085415 (2003).
7. Genet, C., van Exter, M. P. & Woerdman, J. P. Fano-type interpretation of red shifts and red tails in hole array transmission spectra. *Opt. Commun.* **225,** 331–336 (2003).
8. Barnes, W. L., Murray, W. A., Dintinger, J., Devaux, E. & Ebbesen, T. W. Surface plasmon polaritons and their role in the extraordinary transmission of light through periodic arrays of subwavelength holes in a metal film. *Phys. Rev. Lett.* **92,** 107401 (2004).
9. Klein Koerkamp, K. J., Enoch, S., Seqerik, F. B., van Hulst, N. F. & Kuipers, L. Strong influence of hole shape in enhanced transmission through periodic arrays of subwavelength holes. *Phys. Rev. Lett.* **92,** 183901 (2004).
10. Gordon, R. *et al.* Strong polarization in the optical transmission through elliptical nanohole arrays. *Phys. Rev. Lett.* **92,** 37401 (2004).
11. Degiron, A., Lezec, H. J., Yamamoto, N. & Ebbesen, T. W. Optical transmission properties of a single subwavelength aperture in a real metal. *Opt. Commun.* **239,** 61–66 (2004).
12. Schouten, H. F. *et al.* Plasmon-assisted two-slit transmission: Young's experiment revisited. *Phys. Rev. Lett.* **94,** 053901 (2005).
13. Williams, S. M. *et al.* Use of the extraordinary infrared transmission of metallic subwavelength arrays to study the catalyzed reaction of methanol to formaldehyde on copper oxide. *J. Phys. Chem. B* **108,** 11833–11837 (2004).
14. Brolo, A. G., Gordon, R., Leathem, B. & Kavanagh, K. L. Surface plasmon sensor based on the enhanced light transmission through arrays of nanoholes in gold films. *Langmuir* **20,** 4813–4815 (2004).
15. Nahata, A., Linke, R. A., Ishi, T. & Ohashi, K. Enhanced nonlinear optical conversion from periodically nanostructured metal film. *Opt. Lett.* **28,** 423–425 (2003).
16. Luo, X. & Ishihara, T. Surface plasmon resonant interference nanolithography technique. *Appl. Phys. Lett.* **84,** 4780–4782 (2004).
17. Ishi, T., Fujikata, J., Makita, K., Baba, T. & Ohashi, K. Si nanophotodiode with a surface plasmon antenna. *Jpn J. Appl. Phys.* **44,** L364–L366 (2005).
18. Shinada, S., Hasijume, J. & Koyama, F. Surface plasmon resonance on microaperture vertical-cavity surface-emitting laser with metal grating. *Appl. Phys. Lett.* **83,** 836–838 (2003).
19. Bravo-Abad, J., García-Vidal, F. J. & Martín-Moreno, L. Resonant transmission of light through finite chains of subwavelength holes in a metallic film. *Phys. Rev. Lett.* **93,** 227401 (2004).
20. Martín-Moreno, L. & García-Vidal, F. J. Optical transmission through circular hole arrays in optically thick metal films. *Opt. Express* **12,** 3619–3628 (2004).

Acknowledgements

Financial support by the EC under Project Nos. FP6-NMP4-CT-2003-505699 (Surface Plasmon Photonics) and FP6-2002-IST-1-507879 (Plasmo-Nano-Devices) is gratefully acknowledged. Correspondence and requests for materials should be addressed to F.J.G.-V.

Competing financial interests

The authors declare that they have no competing financial interests.